2026 IEEE International Conference on Robotics and Automation (ICRA 2026)
June 1-5, 2026. Vienna, Austria

Direct in-Petri Dish Liquid Droplet Manipulation Based on Microscope and Ultrasonic Phased Transducer Array

Huamin Li and Song Liu*, *Member, IEEE*

***Abstract* — High-precision liquid droplet manipulation is widely used in life science, biomedical engineering, and industry. However, there still lacks a robotic approach supporting the direct in-petri dish manipulation of liquid droplets without the need of additives (such as magnetic beads) or other setup requirements (such as on hydrophobic or conductive surfaces). From the robotics perspective, this challenge concerns with designing an adequate robot end-effector capable of firmly holding and effectively moving droplet on hydrophilic surfaces. In this paper, we propose an automated robotic system for the direct in-petri dish liquid droplet manipulation based on ultrasonic phased transducer array (UPTA) and microscope, which can interact with users to selectively grasp droplet, follow user designated trajectories to transport droplet, and positioning droplet in high precision. The core working mechanism of the proposed system is to precisely generate an inclined single focal point, acting as a noncontact end-effector, inside the droplet under the guidance of microscope, which can induce sufficient hydrodynamic actuation forces on the peripheral contact line of the droplet to keep the droplet moving along the ultrasonic end-effector. Since it is additive free, our system is inherently compatible to medical, chemical and industrial protocols. Details regarding the system design and implementation, the ultrasound focusing strategy, and the visual servo control scheme are elaborated in this paper. Experiments validated the effectiveness of the proposed system.**

I. Introduction

While robotic systems have attained remarkable proficiency in manipulating solid objects spanning from rigid to even ultrasoft materials [1], handling liquid objects with comparable dexterity, autonomy and precision remains a significant and prolonged challenge [2]. For numerous applications in scientific research and industry [3], samples or reagents are commonly in liquid droplet form. Consequently, the development of automated droplet manipulation systems that meet the robotic standards of efficiency, accuracy, and reliability warrants research efforts from robotics community [4-5]. Following this context, the direct in-petri dish droplet manipulation without the need of additives to liquid droplets or specific customization to system setups (basically hydrophobic surfaces) would benefit different fields such as life science, medication, chemistry, and industry [6].

This paper was supported in part by the National Natural Science Foundation of China under Grant 62303321 and T2522022. (Corresponding author: *Song Liu*)

H. Li and S. Liu are with the School of Information Science and Technology, ShanghaiTech University, Shanghai 201210, China. (e-mail: lihm12025, liusong@shanghaitech.edu.cn).

Existing droplet manipulation techniques can be categorized into contact-based [7] and non-contact ones [8]. Contact-based manipulation achieves droplet control via capillary forces [9] or adsorption methods [10], yet it requires strict control of contact force and carries the risk of tool-induced cross-contamination, thus making it unsuitable for microfluidic experiments that demand high purity [11]. In the contrary, non-contact manipulation is extensively studied due to the advantage of minimizing damage and contamination [12-13]. For example, magnetic-based systems operate by introducing magnetic nanoparticles/beads into the liquid droplet, which can then be steered by external magnetic fields [14]. However, this approach suffers from significant limitations, since the introduced nanoparticles can catalyze the reaction of certain reagents due to intrinsic peroxidase-like activity, thereby contaminating the sample. Other non-contact manipulation methods, such as those based on thermal gradients [15], also present challenge such as causing thermal damage to sensitive biological samples like cells and proteins. In contrast, ultrasonic manipulation techniques emerge as a powerful and versatile alternative that overcomes these fundamental limitations [16]. However, reported ultrasonic manipulation methods [17], together with the contact-based or other non-contact methods, necessitate hydrophobic surfaces in their setups in order to minimize the droplet pinning forces for effective droplet actuation, making them hardly compatible to underlying medical, chemical and industrial protocols.

To overcome the shortcomings of reported droplet manipulation techniques, this paper proposes a novel ultrasonic robotic system for the direct in-petri dish liquid droplet manipulation based on ultrasonic phased transducer array (UPTA) and microscope. Our system achieves automated and high precision droplet motion control without the need of additives or other setup requirements. Specifically, the UPTA can generate a configurable inclined single focal point inside the droplet under the guidance of microscope. The inclined focal point, essentially acting as the noncontact end-effector, can induce sufficient hydrodynamic actuation forces on the peripheral contact line of the droplet to move the droplet along the end-effector directly on petri dish surface. The rest of the paper is organized as follows: Section II presents the manipulation system setup and calibration; Section III details the design, configuration and generation method of the ultrasonic end-effector; Section IV elaborates the control scheme for droplet positioning and motion control; Section V shows the experimental results.

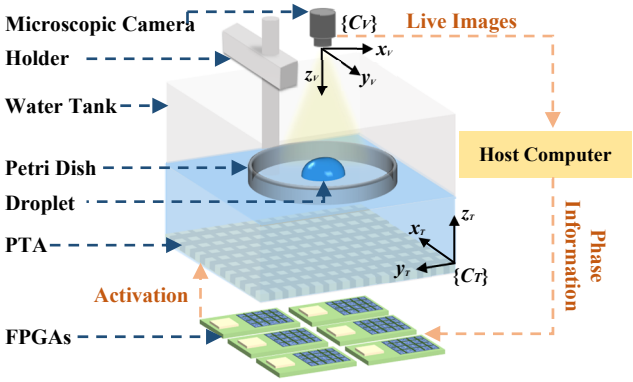

Fig. 1. Schematic illustration of the automated robotic system for the direct in-petri dish liquid droplet manipulation based on ultrasonic phased transducer array (UPTA) and microscope. Note that the used petri dish is made of polystyrene and does not need hydrophobic treatment in advance.

II. System Illustration and Calibration

The liquid droplet manipulation system, as illustrated in Fig. 1, is primarily comprised of an ultrasonic phased transducer array (UPTA), a water tank, a microscopic camera, and a host computer. One laboratorial polystyrene (PS) petri dish can be directly placed right upon the water surface, without the need of hydrophobic treatment in advance, while the distance between the petri dish and UPTA is fixed by the water altitude in the water tank. In this configuration, the petri dish acts as the workspace for all manipulation tasks. Droplets of water, oil, or mixtures, can be transferred to petri dish by classical chemical, industrial, or medical protocols. The host computer localizes the droplets through the visual feedback from the microscope, and calculates the necessary phase information to activate the UPTA, which thereafter generate an ultrasonic end-effector for droplet manipulation. The key setup factor for this liquid droplet manipulation system is the selection of suitable ultrasound frequency so that adequate ultrasound energy can be propagated into the droplet through the petri dish for effective actuation.

To enable vision-based close-loop control, the system must be calibrated in advance to establish the hand-eye relationship between the 2D image plane of the camera and the 3D Cartesian space of the UPTA. This is achieved by calculating the image Jacobian matrix $\boldsymbol{J_v}$, which maps the motion increments in Cartesian space $\{\boldsymbol{Cr}\}$ to the motion increments in image space $\{\boldsymbol{Cv}\}$. To this end, multiple calibration points are selected randomly from workspace with their coordinates in both $\{\boldsymbol{Cr}\}$ and $\{\boldsymbol{Cv}\}$ recorded by referring to a hydrophone. Notably, owing to the fact that droplet manipulation happens directly at the petri dish in our work, the motion increments along the z-axis can be considered to be zero. Therefore, $\boldsymbol{J_v}$ is set to be a 2D matrix, which satisfies

$$\begin{bmatrix} x_{ptc} \\ y_{ptc} \\ z_{ptc} \end{bmatrix} = \begin{bmatrix} x_{ref} \\ y_{ref} \\ z_{ref} \end{bmatrix} + \begin{bmatrix} J_v^{\dagger} \\ 0 \end{bmatrix} \begin{bmatrix} u_{ptc} - u_{ref} \\ v_{ptc} - v_{ref} \end{bmatrix} \tag{1}$$

where $[x_{ptc}, y_{ptc}, z_{ptc}]^{\mathrm{T}}$, $[x_{ref}, y_{ref}, z_{ref}]^{\mathrm{T}}$ and $[u_{ptc}, v_{ptc}]^{\mathrm{T}}$, $[u_{ref}, v_{ref}]^{\mathrm{T}}$ are point coordinates in $\{\boldsymbol{Cr}\}$ and $\{\boldsymbol{Cv}\}$ respectively, with the subscript *ptc* and *ref* referring to hydrophone's needle tip and reference point. Details regarding the calibration procedure can be found in [18].

III. Ultrasonic End-Effector Design, Generation and Configuration for Droplet Manipulation

From the robotics perspective, the implementation of one liquid droplet manipulation system essentially concerns with designing an adequate robot end-effector capable of firmly holding and effectively moving droplet on hydrophilic surfaces (The PS petri dish surface has a contact angle of 90°). In this section, we will introduce the design, configuration and generation method of the ultrasonic end-effector used in this work.

A. Inclined Single Focal Point for Droplet Manipulation

It has been reported from literature that acoustic tweezers generating single focal point to levitate a liquid droplet in air [16] or trap a liquid droplet on super hydrophobic surface [17]. In both scenarios, the applied ultrasound must have a wavelength larger than the size of the liquid droplet so that the droplet can be fully enclosed by the single focal point. Under this circumstance, it is the acoustic radiation force [19] that dominates the dynamics of the liquid droplets. Since acoustic radiation force typically lies in the level of micro-Newtons, it can hardly overcome the resistance force of a droplet resting on an untreated PS petri dish surface. To realize the direct in petri dish droplet manipulation of liquid droplets, we chose a different strategy of focusing ultrasound waves inside the liquid droplet sitting on petri dish. In this case, the applied ultrasound wavelength can be rather smaller than the size of the droplet. By referring to the acoustofluidics theory [20], the focused ultrasound will induce acoustic streaming inside the droplet (Fig. 2(b)), which, consequently, can induce sufficient hydrodynamic actuation forces on the peripheral contact line of the droplet to hold and mobolize the droplet along the focused ultrasound.

To further enhance the actuation force, we use an inclined single focal point (ISFP) as the ultrasonic end-effector for liquid droplet manipulation in this work (Fig. 2(a)), where the inclination direction always points towards droplet motion direction through dynamically modulating the UPTA.

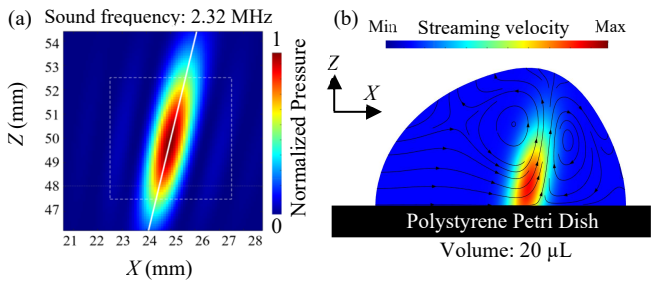

Fig. 2. COMSOL simulation results of the used ultrasound end-effector. (a) The pressure profile of ISFP for droplet manipulation at XOZ plane; (b) the acoustic streaming inside droplet induced by ISFP at XOZ plane.

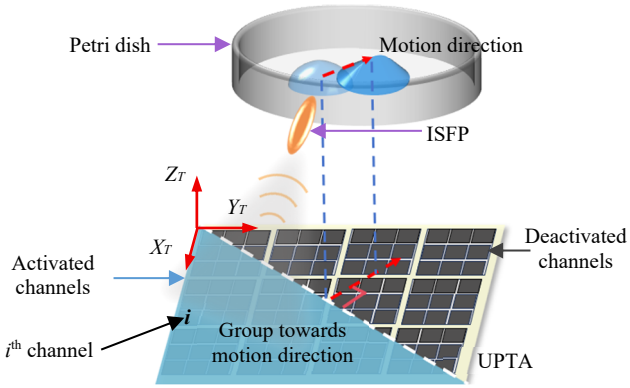

Fig. 3. Schematic illustration of generating an inclined single focal point (ISFP) as ultrasonic end-effector for droplet manipulation from an ultrasonic phased transducer array (UPTA) based on droplet motion direction.

B. Generation and Configuration of ISFP

The generation of an ISFP inside a droplet is realized through the real-time and trajectory-dependent modulation of the UPTA's active channels, conceptually illustrated in Fig. 3. Specifically, to generate an ISFP given its coordinate in $\{\boldsymbol{C_T}\}$ based on the droplet position from microscope feedback, the UPTA's channels are divided into two separate groups by a line (the white dashed line in Fig. 3) perpendicular to the instantaneous motion direction (red dashed arrow in Fig. 3) defined from the motion trajectory. Only the channels in the group towards the droplet motion direction are activated to emit sound waves, whose phase are calculated by

$$\phi_i = 2\pi - \mathrm{mod}\left(-\frac{2\pi}{\lambda}\| \boldsymbol{x}_i - \boldsymbol{P}_{target} \|_2, 2\pi\right) \tag{2}$$

where $\boldsymbol{x}_i$ is the coordinate of the i^{th} channel in $\{\boldsymbol{C_T}\}$, $\boldsymbol{P}_{target}$ is the ISFP coordinate in $\{\boldsymbol{C_T}\}$, and λ is the wavelength. Fig. 2 (a) shows the ISFP at $\boldsymbol{P}_{target}$ = [25, 25, 50]$^{\mathrm{T}}$ mm simulated by COMSOL with the UPTA parameters given in Section V.A.

Note that, while the ISFP generation method ensures the direction of the driving force pointing towards the droplet motion direction, the inclination angle of ISFP and the applied focal pressure do not necessarily to be constant. Actually, they change dynamically as the droplet moves across the workspace, as the number of activated channels varies with the droplet position. The applied focal pressure, which is mostly proportional to the number of activated channels, is also a key configuration parameter for effective manipulation. For lower focal pressure, the induced hydrodynamic actuation force is insufficient to overcome the resistance force from the petri dish surface, and the droplet remains stationary. Conversely, if the applied focal pressure becomes too high, the acoustic streaming is so fierce that the droplet turns out to be unstable and will be ejected away from petri dish surface. Therefore, to achieve stable droplet manipulation, the system must ensure that the applied focal pressure remains within an effective range. In Section V.B, we characterized the necessary focal pressure for successful droplet manipulation directly in petri dish surface.

IV. Automated Liquid Droplet Manipulation

A. Droplet Localization and Feature Extraction

The ISFP generated by UPTA actuates the droplet on petri dish surface in a step-by-step mode. Once the step size is larger than droplet size, the droplet will lose controllability. This essentially concerns with the stability problem of one manipulation task. On the other hand, to move a droplet following one user-designated trajectory for customized purposes such as obstacle crossing, the position of the droplet during motion should also be well controlled. Therefore, closed-loop control is necessary for robust droplet manipulation, and reliable visual feedback is adopted as a sensory input in our system. The visual localization of droplet is realized through a streamlined image processing pipeline which extracts the geometric center of droplet on images grabbed from the microscope. The pipeline begins by first transforming the input image from RGB to HSV format to achieve robust segmentation against illumination variations. A binary image is then generated by applying a color threshold, identifying pixels that correspond to the droplet. To ensure the integrity of the segmented region on image, a morphological closing operation is subsequently performed to eliminate internal voids and smooth the object's boundary. Following this refinement, contours are extracted from the binary image. After filtering out spurious detections based on a minimum area criterion, the image moments of each valid contour are computed. The precise droplet position in the image plane is then determined by calculating the centroid from these moments, which can then be converted to $\{\boldsymbol{C_T}\}$ by leveraging the calibrated pseudo image Jacobian matrix $\boldsymbol{J_v}^*$.

B. Motion Control for Positioning and Trajectory Tracking

As mentioned in last section, the ISFP generated by UPTA actuates droplet on petri dish surface in a step-by-step mode. The motion control for droplet manipulation concerns with generating the ISFP at the right position for next control step. For both the droplet manipulation task of positioning and trajectory tracking, a coordinate sequence for ISFP should first be planned in advance based on the principle that the step size between two adjacent coordinates should be less than the droplet radius. Quite smaller step size will of course increase the manipulation stability, but will also significantly decrease the manipulation efficiency (given a fixed ISFP updating frequency from the UPTA). Therefore, the step size should be carefully selected, balancing controllability and efficiency. By resorting to closed-loop visual servo control, we can localize the droplet and exam whether the droplet will lose controllability for the next control step by checking whether the distance between the droplet and the coming ISFP coordinate is larger than droplet radius. In this section, the motion controllers for precision positioning and trajectory planning are given. For clarity, positioning task concerns with moving a droplet from its original position to a target position with a straight-line motion trajectory, while trajectory tracking tasks means moving a droplet along a pre-planned or user-designated trajectory.

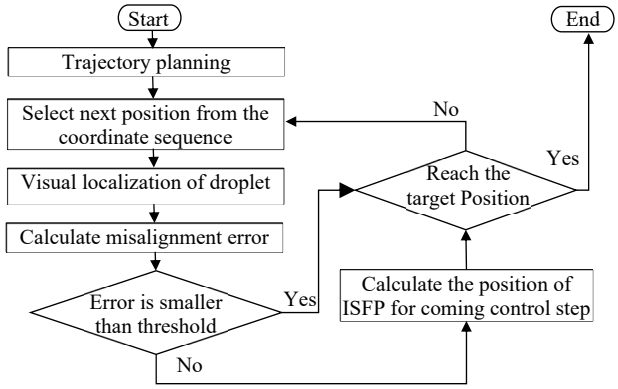

Fig. 4. The control flowchart for trajectory tracking task.

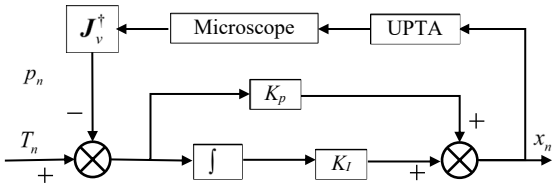

Fig. 5. The control diagram for trajectory tracking task.

To achieve stable and smooth trajectory tracking, a Proportional-Integral (PI) controller is adopted to regulate the position of ISFP, which is given as

$$\begin{cases} \boldsymbol{x}_n = K_p(\boldsymbol{p}_n - \boldsymbol{T}_n) + K_I \sum_{i=1}^{n} (\boldsymbol{p}_i - \boldsymbol{T}_i) \text{ if } \|\boldsymbol{x}_n - \boldsymbol{p}_n\|_2 < stepsize \\ \boldsymbol{x}_n = \boldsymbol{x}_{n-1} + \dfrac{\boldsymbol{T}_n - \boldsymbol{x}_n}{\|\boldsymbol{T}_n - \boldsymbol{x}_n\|_2} \times stepszie \quad \text{if } \|\boldsymbol{x}_n - \boldsymbol{p}_n\|_2 > stepsize \end{cases} \tag{3}$$

where $\boldsymbol{p}_n$ represents the current droplet position obtained from the visual localization pipeline in Section IV.A and the pseudo image Jacobian matrix $\boldsymbol{J}_v^\dagger$ in Eq. (1), $\boldsymbol{T}_n$ represents the position for the n^{th} control step from the planned coordinate sequence (*stepsize* represents the distances between two adjacent coordinates), and $\boldsymbol{x}_n$ represents the position of ISFP. The controller is designed by checking whether the distance between next ISFP position and current droplet position is larger than *stepsize*. If yes, the controller moves the droplet towards planned position by step size; otherwise, the next ISFP position will be calculated by compensating the systematic misalignment errors during trajectory tracking. Fig. 4 and Fig. 5 shows the corresponding control flowchart and control block diagram respectively.

Positioning controller focuses on eliminating the position misalignment error between droplet and the target position, which updates ISFP position iteratively to compensate the observed misalignment error, where an integral controller is adopted, given as

$$\boldsymbol{x}_n = \boldsymbol{x}_{n-1} + K_{IT}\left(\boldsymbol{p}_n - \boldsymbol{T}_n\right) \tag{4}$$

where K_{IT} is the proportional parameter. This controller continuously adjusts the ISFP position until the misalignment error converges below a predefined threshold.

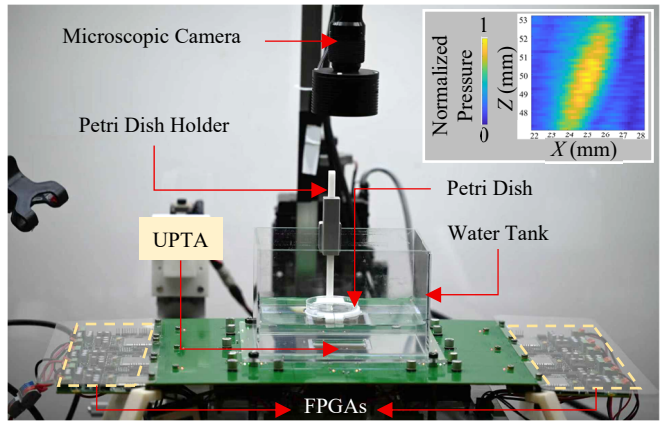

Fig. 6. The prototyped direct in-petri dish liquid droplet manipulation system. The UPTA was fabricated from 1 mm thick monolithic PZT ceramic. Laboratory-used polystyrene petri dish can be place right on water surface. The inset shows the pressure profile of the generated ISFP at XOZ plane with the same simulation parameters in Fig. 2 (a).

V. Experiments and Results

A. Liquid Droplet Manipulation System Prototyping

The prototyped liquid droplet manipulation system is shown in Fig. 6. The UPTA consists of 2500 independently controllable channels, with each channel in size of 800 × 800 μm. The UPTA was fabricated from 1 mm thick lead zirconate titanate (PZT-5A) ceramic, with 1 mm pitch size. The UPTA is driven by 2.32 MHz square waves at 10 Volts by a customized driver board equipped with six field programmable gate arrays (FPGAs). The FPGAs receive phase information from the host computer through controller area network (CAN) bus. The established system allows real-time generation of ISFP with maximum updating frequency of 11 Hz. The used microscopic camera is Prosilica GC2450 microscopic camera with Navitar zoom lens, which captures images of the workspace at 15 FPS with a resolution of 2448 × 2050 pixels. The UPTA is housed in an acrylic water tank filled with deionized water, which serves as the ultrasonic coupling medium. The water altitude was set to be 50 mm. The 1mm thick PS petri dish is place right upon the water surface without any treatment in advance. The pseudo image Jacobian matrix of the system was calibrated with a 0.2 mm needle hydrophone (Precision Acoustics, NH0200) as

$$J_v^\dagger = \begin{bmatrix} -15.5906 & 1.0471 \\ -1.1219 & -15.5411 \end{bmatrix} \mu m / pixel \tag{4}$$

with $[x_{ref}, y_{ref}, z_{ref}]^T = [25, 25, 50]^T$ mm.

B. Ultrasonic end-effector characterization

The inset of Fig. 6 shows the pressure profile of an ISFP at the XOZ plane generated with the liquid droplet manipulation system at $[25, 25, 50]^T$ mm in $\{\boldsymbol{Cr}\}$, which was obtained by rater-scanning with NH0200 need hydrophone. It can be seen that the experimental results well coincide with the simulation results in Fig. 2 (a) under the same ultrasound frequency and setup parameters, demonstrating the effectiveness of the system for droplet manipulation.

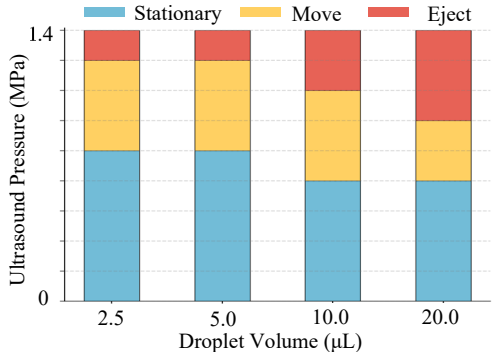

Fig. 7. Droplet motion behavior characterization at different ultrasound pressures under ISFP.

We then characterized the motion behaviors of droplets under the actuation of ISFP at different ultrasound pressure. As discussed in Section III.B, one droplet shows three distinct behaviors under different ultrasound pressure actuation, such as keeping stationary, moving over the surface, or being ejected from the petri dish surface, which was also experimental valiated. From Fig. 7, for droplets of different volumns, the appliable ultrasound pressure realizing effective and stable droplet manipulation varies. This could be potentially explained by referring to the fluid-solid-acoustic coupling theory [21]. We would to emphasize that, the prototyped system is capable of effectively manipulating droplets ranging from several to tens of micro-liters, which are common volumns in chemistry and medicine analysis.

C. Droplet Positioning Experiments

A series of experiments were conducted to quantitatively evaluate the droplet positioning performance of our system. The positioning performance with and without closed-loop control strategies was also compared to highlight the superiority of automated droplet manipulation technique. Specifically, the droplet positioning experiments moved a droplet from a starting position to a designated target point. This task was executed multiple times to assess repeatability, and consisted of two stages. In first stage, the open-loop control strategy was employed. The system pre-calculated the overall phase information required to actuate UPTA to move the ISFP from the start to the target position along a straight-line trajectory and executed without any feedback. While this stage is straightforward, the final position of the droplet is susceptible to drift and cumulative errors, leading to noticeable deviations from the target. In the second stage, the visual servo control strategy for positioning given in Section IV.B was enabled, where the integral parameter K_{IT} in Eq. (4) was set to be 0.2. This droplet positioning task finished once the position misalignment error got smaller than a threshold ($0.05 \times r$, i.e., 5 percent of droplet radius). Fig. 9 shows the converging positioning error during the second stage for a 20 μL droplet positioning task. Note that, the closed-loop positioning control started when the misalignment error is less than droplet radius r. As can be seen that closed-loop visual servo control significantly enhanced the droplet positioning performance.

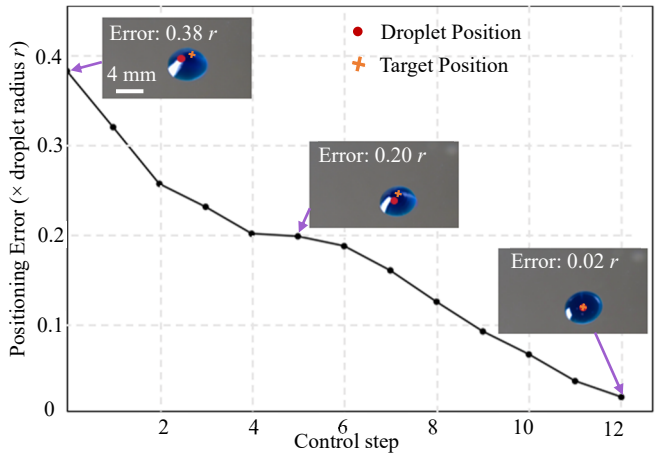

Fig. 8. The misalignment error during one droplet positioning task.

Liquid droplets are different from solid objects in terms of fluidity-induced deformability; In addition, the resistance force imposed by petri dish is sensitive to surface properties. Consequently, the droplet motion shows hysteresis particularly when the droplet motion direction changes, agreeing with the contact angle hysteresis phenomenon [22]. Further, as discussed in Section III.B, the applied focal pressure and the inclination angle of ISFP changes under UPTA with droplet position, leading to the morphological change of droplet with control step. Therefore, as shown in Fig. 8, it took 12 steps to converge the misalignment error to be less than $0.05 \times r$. Also, due to these reasons, we used the ratio between the misalignment error and droplet radius as the metric to end the positioning task and evaluate positioning performance.

Table I shows the repetitive positioning experiment results with different droplet volumes. As can be seen that, with and without closed-loop visual servo, the droplet positioning task shows significant performance difference. With our proposed visual servo scheme, the droplet positioning error is one order of magnitude smaller (from $0.3393 \times r$ to $0.0393 \times r$ for 5 μL droplets, and $0.3631 \times r$ to $0.0351 \times r$ for 10 μL droplets on average), highlighting the high reliability of the proposed system for the direct in-petri dish droplet manipulation. Meanwhile, Table I also demonstrate the high repeatability of the system in positioning task against droplet volumes.

TABLE I. POSITIONING ERRORS OF REPETITIVE EXPERIMENTS OVER DIFFERENT DROPLET VOLUMES

	Droplet volume: 5 μL		Droplet volume: 10 μL	
Exp. No	Without closed-loop visual servo (× *radius*)	With closed-loop visual servo (× *radius*)	Without closed-loop visual servo (× *radius*)	With closed-loop visual servo (× *radius*)
1	0.3538	0.0155	0.3826	0.0313
2	0.3393	0.0499	0.3606	0.0366
3	0.3605	0.0437	0.3902	0.0253
4	0.3122	0.0159	0.3612	0.0389
5	0.3309	0.0457	0.3209	0.0435
Avg.	0.3393	**0.0393**	0.3631	**0.0351**

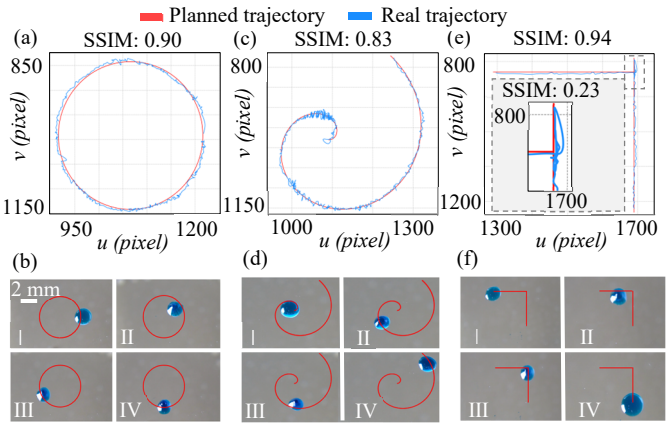

Fig. 9. Trajectory tracking experiments over circular (a), spiral (c) and zigzag (e) trajectories. The (b), (d) and (e) show snapshots during tracking tasks.

D. *Trajectory Tracking Experiments*

With the established droplet manipulation system, trajectory tracking experiments were also conducted with circular, spiral and zigzag trajectories with the proposed visual servo scheme in Section IV.B. The proportional and integral parameters in Eq. (3) were set to be 0.2 and 0.05 respectively, while the step size for trajectory planning was 80 μm. In all trajectory tracking experiments, 3.5 μL water droplets dyed in blue color were used for better visualization. These trajectories were selected to systematically evaluate different aspects of motion control strategy during trajectory tracking, including curvature adaptation, spatial accuracy, and direction reversal.

Fig. 9 illustrates the trajectory tracking experiment results. As can be seen, evaluated by the structural similarity index measure (SSIM), the implemented droplet motion trajectories highly coincide with the ideally designed trajectories, achieving a trajectory similarity of 0.9 on average. Theoretically and experimentally, it is easier to precisely track straight lines than curvatures, which was also confirmed by the tracking performance in the corner of zigzag trajectory. The SSIM in the zigzag corner zone (see inset of Fig. 9 (e)) was only 0.23, drastically smaller than the SSIM on the overall trajectory. This observation agrees to the contact angle hysteresis phenomenon [22], which leads to the motion hysteresis characteristics similar to classical mechanical transmission systems.

E. *Application of Automated Liquid Droplet Manipulation*

To show the application potential of the proposed droplet manipulation technique, a droplet-based chemical reaction task involving particle collection was designed in petri dish. The task concerns with moving a 4 μL phenolphthalein droplet towards a 4 μL sodium hydroxide (NaOH) droplet, through following a user-designated trajectory which circumvents obstacles (Fig. 10 (a)). The trajectory passes through a solid particle so that the particle will be picked and moved towards destination. Fig. 10 (b)-(d) show the snapshots captured during droplet motion along the trajectory. Once the two droplets merged (Fig. 10 (e)), chemical reaction was triggered immediately, and the droplet turned to be pink.

The successful implementation of this task highlights the significance of realizing the direct in-petri dish droplet manipulation, and also demonstrates the dexterity, flexibility, and applicability of the proposed system in chemistry, medication, and industry. Users only need to transfer droplets into a PS petri dish and place the petri dish upon water surface. The system would help to substantially improve the operation efficiency and precision. Our future research efforts will focus on investigating the underlying dynamics of droplet motion under ultrasound actuation.

VI. Conclusion

In this work, we proposed an ultrasonic robotic system for the direct in-petri dish droplet manipulation. The system primarily consists of an ultrasonic phased transducer array and a microscope. Closed-loop visual servo control scheme is proposed for droplet positioning and trajectory tracking. Through series of quantitative experiments, the performance of the system was systematically evaluated and demonstrated. The proposed system shows adequate combability to existing chemical, medical and industrial protocols. It should be noted that, only the readily usable 1 mm thick petri dishes made of polystyrene material are supported by our prototyped system, since acoustic impedance matching is critical for the effective transmission of ultrasound energy from ultrasound transducer to the droplet. For petri dishes made of other materials, such as glass, polypropylene or cellulose acetate, the thickness of the petri dish or the applied ultrasound frequency should be dedicatedly selected.

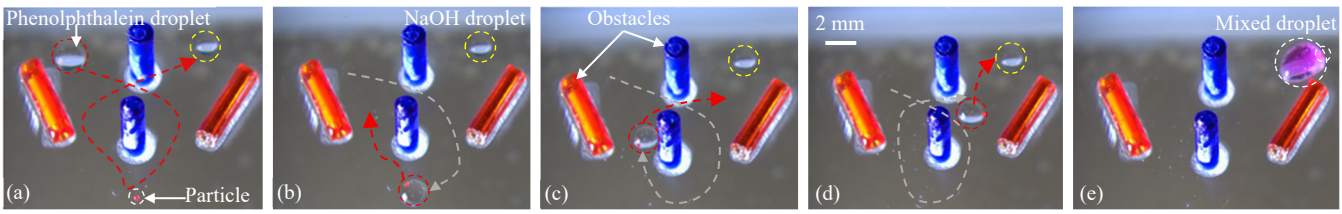

Fig. 10. Demonstration of an automated chemical reaction experiment involving particle collection. (a) The initial experimental setup, showing the user-designated trajectory, a phenolphthalein droplet, a target particle, obstacles (in red and blue color), and a sodium hydroxide (NaOH) droplet. (b) The phenolphthalein droplet is transported to the particle's location. (c) The droplet, now carrying the particle, is moving around a cylindrical obstacle. (d) The particle-laden droplet completes the trajectory, navigating around the obstacles to approach the NaOH droplet. (e) The droplets merged, and the successful chemical reaction is indicated by the resulting pink color of the final combined liquid containing the transported particle.

REFERENCES

[1] J. Zhu, A. Cherubini, C. Dune, D. Navarro-Alarcon, F. Alambeigi, D. Berenson, *et al.*, "Challenges and outlook in robotic manipulation of deformable objects," *IEEE Robot. Autom. Mag.*, vol. 29, no. 3, pp. 67-77, 2022.

[2] A. Chiolerio and M. B. Quadrelli, "Smart fluid systems: the advent of autonomous liquid robotics," *Adv. Sci.*, vol. 4, no. 7, p. 1700036, 2017.

[3] T. S. Kaminski, and P. Garstecki, "Controlled droplet microfluidic systems for multistep chemical and biological assays," *Chem. Soc. Rev.*, vol. 46, no. 20, pp. 6210-6226, 2017.

[4] R. Zhang, C. Zhang, X. Fan, C. C. Au Yeung, H. Li, H. Lin, and H. C. Shum, "A droplet robotic system enabled by electret-induced polarization on droplet," *Nat. Commun.*, vol. 15, no. 1, p. 6220, 2024.

[5] G. Z. Yang, J. Bellingham, P. E. Dupont, P. Fischer, L. Floridi, R. Full, *et al.*, "The grand challenges of science robotics," *Sci. Robot.*, vol. 3, no. 14, p. eaar7650, 2018.

[6] Z. Tian, Z. Wang, P. Zhang, T. D. Naquin, J. Mai, Y. Wu, *et al.*, "Generating multifunctional acoustic tweezers in Petri dishes for contactless, precise manipulation of bioparticles," *Sci. Adv.*, vol. 6, no. 37, p. eabb0494, 2020.

[7] Kim, H., Roh, H., Kim, H., and Park, J. K., "Droplet contact-based spheroid transfer technique as a multi-step assay tool for spheroid arrays," *Lab Chip*, vol. 21, no. 21, pp. 4155-4165, 2021.

[8] Z. Yang, H. Li, G. Chen, J. Liang, and X. Zhang, " Non-contact ultrasonic manipulation for targeted micro-droplet merge by using a flat–sharp cantilever," *Sens. Actuators A, Phys.,* vol. 345, 2022, Art. no. 113764.

[9] X. Liu, *et al.*, "Capillary tweezer for programmable droplet manipulation," *Sens. Actuators B: Chem.*, vol. 370, p. 132380, 2022.

[10] H. Li, A. Li, Z. Zhao, L. Xue, M. Li, and Y. Song, "Precise droplet manipulation based on surface heterogeneity," *Acc. Mater. Res.*, vol. 2, no. 4, pp. 230-241, 2021.

[11] J. Autebert, B. Coudert, J. Champ, L. Saias, E. T. Guneri, R. Lebofsky, *et al.*, "High purity microfluidic sorting and analysis of circulating tumor cells: towards routine mutation detection," *Lab Chip*, vol. 15, no. 9, pp. 2090-2101, 2015.

[12] I. I. I. Al-Nuaimi, M. N. Mahyuddin, and N. K. Bachache, "A non-contact manipulation for robotic applications: A review on acoustic levitation," *IEEE Access*, vol. 10, pp. 120823-120837, 2022.

[13] N. Tanaka, Y. Haruzono, H. Nasu, Y. Nakanishi, J. Takahara, A. Awazu, and Y. Tanaka, "Contamination-free non-contact wettability assessment system," *ROBOMECH Journal.*, vol. 4, no. 1, p. 21, 2017.

[14] A. Li, H. Li, Z. Li, Z. Zhao, K. Li, M. Li, and Y. Song, "Programmable droplet manipulation by a magnetic-actuated robot," *Sci. Adv.*, vol. 6, no. 7, p. eaay5808, 2020.

[15] Z. Z. Liu, C. Zhang, T. Wen, H. Z. Li, W. P. Gao, X. K. Wang, *et al.*, "Photo-responsive droplet manipulation slippery lubricant-infused porous surface with ultra-high durability," *Chin. Phys. B*, vol. 32, no. 11, p. 116801, 2023.

[16] Y. Koroyasu, T. V. Nguyen, S. Sasaguri, A. Marzo, I. Ezcurdia, Y. Nagata, *et al.*, "Microfluidic platform using focused ultrasound passing through hydrophobic meshes with jump availability," *PNAS Nexus*, vol. 2, no. 7, 2023, Art. no. pgad207.

[17] Z. Yuan, C. Lu, C. Liu, X. Bai, L. Zhao, S. Feng, and Y. Liu, "Ultrasonic tweezer for multifunctional droplet manipulation," *Sci. Adv.*, vol. 9, no. 16, p. eadg2352, 2023.

[18] M. Wang, S. An, Z. Sun, J. Li, Y. Wang, and S. Liu, "Selective, robust and precision manipulation of particles in complex environments with ultrasonic phased transducer array and microscope," *IEEE Trans. Robot.*, vol. 40, no. 4, pp. 4586-4598, Apr. 2024.

[19] K. Dholakia, B. W. Drinkwater, and M. Ritsch-Marte, "Comparing acoustic and optical forces for biomedical research," *Nat. Rev. Phys.*, vol. 2, no. 9, pp. 480-491, 2020.

[20] T. Godary, B. Binkley, Z. Liu, O. Awoyemi, A. Overby, H. Yuliantoro, *et al.*, "Acoustofluidics: Technology Advances and Applications from 2022 to 2024," *Anal. Chem.*, vol. 97, no. 13, pp. 6847-6870, 2025.

[21] Müller, S., Becker, S., Biermeier, T., Grabinger, J., and Kaltenbacher, M., "Fluid-Structure-Acoustic Coupling Related to the Flow over Rigid and Flexible Plate Structures," presented at the DAGA 2010, Berlin, Germany, 2010.

[22] P.G. de Gennes, F. Brochard-Wyart, and D. Quéré, *Capillarity and Wetting Phenomena: Drops, Bubbles, Pearls, Waves*. New York, NY, USA: Springer-Verlag, 2004.